Influence of Friction Stir Welding Parameters and TiB_2 Content on Tensile Properties and Weld Nugget Hardness of AA7075 Composites: Taguchi L27 Optimization

[1]*Thiagarajan Chandrasekaran, [2]P. Vimalnathan, [3]D.Madhesh, [4]V. Vimala, [5]N. Viswanathan

[1]*Professor, Department of Mechanical Engineering, Aarupadai Veedu Institute of Technology, Vinayaka Mission's Research Foundation (DU), Tamil Nadu, India

[2]Department of Robotics and Automation, Rajalakshmi Engineering College, Thandalam, Tamil Nadu, India

[3]Professor, Department of Mechanical Engineering, Academy of Maritime Education and Training (AMET) Deemed to be University, Chengalpattu, Tamil Nadu, India

[4]Department of Robotics and Automation, Erode Sengunthar Engineering College, Thuduppathi, Tamil Nadu, India.

[5]Assistant Professor, Department of Mechanical Engineering, Nandha College of Technology, Perundurai, Erode, Tamil Nadu, India

Email ID: [1]*munshianiketprakashrao@gmail.com, [2]vimalanathan.p@rajalakshmi.edu.in, [3]madhesh.d@ametuniv.ac.in

Abstract

This study investigates the addition of friction stir welding (FSW) process parameters on mechanical characteristics of AA7075 aluminium matrix composites reinforced by titanium diboride (TiB_2) particles. AA7075/TiB_2 composites with 3, 6, and 9 wt.% reinforcement was fabricated by stir-casting technique and subsequently joined through FSW. A Taguchi L27 orthogonal array was employed to evaluate four independent factors: welding speed (30–70 mm/min), tool rotational speed (900–1300 rpm), TiB_2 reinforcement content (3–9 wt.%) and axial load (3–7 kN). Percentage elongation (PE), Ultimate tensile strength (UTS) and weld nugget hardness (WNH) were considered as the mechanical responses. Taguchi signal-to-noise (S/N) ratio analysis and analysis of variance (ANOVA) were performed to determine parameter significance and identify the preferred welding conditions. ANOVA showed tool rotational speed were dominant factor affecting UTS (60.87%) and PE (43.27%), whereas TiB_2 content contributed most significantly to WNH (73.83%). The fitted models achieved coefficients of determination (R^2) of 98.26%, 96.61%, and 97.97% for UTS, PE, and WNH, respectively. The preferred conditions for maximizing UTS were 1100 rpm, 50 mm/min, 5 kN, and 6 wt.% TiB_2, yielding a predicted strength of 497.38 MPa. Maximum predicted PE (8.21%) was obtained at 1100 rpm, 50 mm/min, 5 kN, and 3 wt.% TiB_2, while the highest predicted WNH (193.03 HV) corresponded to 1100 rpm, 50 mm/min, 7 kN, and 9 wt.% TiB_2. The findings demonstrate that the preferred axial load and reinforcement concentration depend on the mechanical response, highlighting the effectiveness of Taguchi-based optimization for selecting FSW conditions in AA7075/TiB_2 composites.

Keywords: Friction stir welding, Stir casting, Welding speed, Tensile strength, Optimization, ANOVA

1. Introduction

Aluminium alloys are widely employed in aerospace, automotive, and structural applications due to their lightweight nature, high strength-to-weight ratio, and excellent corrosion resistance. Their mechanical and tribological properties can be further enhanced through alloying, heat treatment, and reinforcement techniques. These characteristics make aluminium alloys promising materials for advanced engineering and high-performance

applications. AA6063 aluminium alloy reinforced with 2–6 wt.% TiB_2 and 2 wt.% graphite was fabricated through stir casting to improve mechanical and tribological properties. The optimum composition containing 4 wt.% TiB_2 and 2 wt.% graphite achieved a tensile strength of 133.67 MPa, hardness of 62.1 BHN, and wear rate of 2.63×10^{-4} mm^3/Nm (Agrawal & Srivastava, 2024b). In-situ A356–TiB_2 aluminium composites were investigated to evaluate mechanical characteristics and EDM machinability. The composites exhibited 251 MPa tensile strength, 120 HV microhardness, and a maximum material removal rate of 60.18 mg/min, with ANOVA identifying discharge current as the dominant parameter (Chinnathambi et al., 2026). Friction stir welding of AA6061-T6 and AA7075-T6 alloys was examined using different tool pin geometries to enhance joint quality. The hexagonal pin profile at 1200 rpm achieved a maximum tensile strength of 608.12 MPa (Manikandan et al., 2025).

Sustainable fabrication of bimetallic tubes was explored using AA7075 and AA2024 aluminium chips through single-step friction stir extrusion. The optimized process produced defect-free bonding interfaces with an average grain size of 4.6 μm and maximum hardness of 175 HV, demonstrating effective material consolidation (Puleo et al., 2026). Pinless friction stir spot welding of 3 mm-thick AA7075-T6 aluminium alloy was investigated using gamma and spiral shoulder groove geometries. The spiral tool produced a larger effective weld width of 419–852 μm, while microhardness ranged from 201–215 HV near the weld center and 150–162 HV in the heat-affected zone (Türkkan, 2026).

Dry turning characteristics of AA7075 reinforced with 15 wt.% SiC particles were examined by varying cutting speed, feed rate, depth of cut, and tool nose radius. RSM, desirability analysis, and genetic algorithms were employed to minimize tangential, feed, and radial cutting forces, with genetic algorithm optimization providing improved cutting-force reduction (Bhushan, 2023). Powder-mixed electrical discharge machining was employed to improve the machinability of AA7075/B_4C and AA7075/B_4C–SiC composites using conductive graphite powder. Taguchi L18 optimization identified 10% reinforcement, 8 A discharge current, and 150 min sintering time as the optimum combination for material removal rate (Keskin et al., 2025). Hybrid AA7075 aluminium composites reinforced with 4 wt.% Si_3N_4 and 2–6 wt.% TiB_2 were fabricated through liquid-state stir casting. The optimum composite containing 6 wt.% TiB_2 exhibited improvements of 59.36% in tensile strength, 95.59% in Brinell hardness, and 49.33% in flexural strength compared with the base alloy (Agrawal & Srivastava, 2024a). AA7075 hybrid composites reinforced with 2 wt.% SiC and 1–3 wt.% WC were fabricated through stir casting. Taguchi optimization revealed that sliding distance was the dominant factor influencing wear (64–82%), followed by applied load and sliding speed (Alam & Singh, 2026).

MIG welding of AA7075 aluminium alloy were optimized by Taguchi and grey relational analysis. Welding current predominantly influenced bead penetration, while shielding gas flow rate significantly affected microhardness (Sharma et al., 2026a). Femtosecond laser surface processing of pure aluminium, AA6061, AA7075, and Scalmalloy was studied to investigate material removal behavior. A 4 W, 400 fs pulse laser operating at frequencies up to 1 MHz produced a maximum ablation depth of 4.1 μm in pure aluminium, demonstrating alloy-dependent surface modification (Cholkar et al., 2026). AA7075 aluminium alloy friction stir welding parameters were optimized through an integrated ANN–GA framework using 27 experimental trials. The predictive models achieved R^2 values above 0.94 and 0.96 for tensile strength and hardness, respectively, while optimized conditions produced 345.76 MPa tensile strength and 143.41 HV maximum hardness (Abouhabaga & El Shrief, 2026). MIG welding of AA7075 aluminium alloy was evaluated by varying welding

current (110–130 A), welding speed (4–6 mm/s), and shielding gas flow rate (17–23 L/min). Taguchi-based grey relational analysis identified welding current as the dominant factor for bead penetration, while gas flow rate significantly influenced microhardness (Sharma et al., 2026b). Al2024 aluminium matrix composites reinforced with TiB_2 particles were investigated to optimize tribological performance using the Grey–Taguchi approach. The optimum parameters of 9 wt.% TiB_2, 10 N load, 2 m/s sliding velocity, and 1000 m sliding distance were identified and validated experimentally (Dey et al., 2022).

Al7075 aluminium composites containing 3, 6, and 9 wt.% TiB_2 were fabricated using stir casting to enhance mechanical and wear resistance properties. The 9 wt.% TiB_2 composite achieved an 11.94% increase in tensile strength, while ANOVA identified reinforcement content as the dominant contributor to wear rate (48.43%) and coefficient of friction (37.68%) (Suhas et al., 2025). TiB_2 nanoparticles were introduced into AA2024 aluminium alloy during laser powder bed fusion to promote grain refinement and suppress hot cracking. The resulting composite developed refined equiaxed grains and achieved an ultimate tensile strength of approximately 502 MPa with 9.9% fracture elongation (Rong et al., 2027). AlSi10Mg aluminium alloy was reinforced with 2 wt.% $AlCoCrFeNi_{2.1}$ high-entropy alloy and 0.1 wt.% TiB_2 through laser powder bed fusion. The hybrid composite exhibited a maximum tensile strength of 516.9 MPa and elongation of 4.2%, while annealing at 300°C for 1 h increased elongation to 8.25% (Chen et al., 2026). AA7075 aluminium alloy was surface-modified using WS_2/Cu through electro-discharge alloying. Taguchi L9 optimization was employed to investigate the effects of normal load, sliding speed, and sliding time on wear rate and coefficient of friction (Senthilkumar et al., 2026).

Novelty of present study lies at systematic evaluation and response-specific optimization of friction stir welding parameters for AA7075 aluminium matrix reinforced with different concentrations of TiB_2 particles. Unlike investigations focusing on individual welding parameters or a single mechanical property, this study employs a Taguchi L27 orthogonal array to simultaneously examine the effects of welding speed, tool rotational speed, TiB_2 reinforcement content and axial load, on percentage elongation, weld nugget hardness and ultimate tensile strength. Integration of Taguchi signal-to-noise ratio analysis with ANOVA enables quantitative identification of dominant parameters governing each mechanical response. A key finding is the distinct influence of reinforcement concentration on joint properties, with 6 wt.% TiB_2 preferred for tensile strength, 3 wt.% for elongation, and 9 wt.% for weld nugget hardness. Furthermore, the identification of a common preferred rotational speed of 1100 rpm and welding speed of 50 mm/min, together with response-dependent axial loads and reinforcement concentrations, provides a practical framework for selecting welding conditions according to the desired mechanical performance of AA7075/TiB_2 composite joints.

2. Materials and Methodology

2.1. Fabrication and characterization of AA7075/TiB_2 composites

AA7075 was selected as the matrix material, while titanium diboride (TiB_2) particles were employed as ceramic reinforcement for composite fabrication. The stir-casting technique was adopted to prepare AA7075/TiB_2 composites with reinforcement concentrations of 3, 6, and 9 wt.%. AA7075 alloy was cleaned to remove surface contaminants before being introduced into the crucible of an electrically heated stir-casting furnace. Chemical composition of the AA7075 aluminium alloy matrix were presented in Table 1.

Table 1. Chemical composition of AA7075 aluminium alloy matrix (wt.%).

Element	Mg	Si	Fe	Mn	Cu	Cr	Zn	Ti	Al
Wt.%	2.50	0.20	0.30	0.10	1.60	0.23	5.60	0.05	Balance

The alloy was heated until a homogeneous molten state was obtained. The TiB_2 particles were preheated before incorporation into the aluminium melt to reduce thermal differences and facilitate particle addition. A mechanical stirrer was used to generate a vortex in the molten alloy, and predetermined quantities of TiB_2 particles were gradually introduced according to the required reinforcement concentration. Stirring was continued to promote particle dispersion throughout the aluminium matrix. The composite melt was subsequently transferred into a preheated metallic mould and allowed to solidify. The resulting castings were removed and machined into rectangular plates measuring 100 × 50 × 5 mm for friction stir welding experiments.



Fig. 1. Fabricated AA7075/TiB_2 stir-cast composite plates prepared for friction stir welding.

The microstructural characteristics of the fabricated composites was investigated using SEM. The examination included the unreinforced AA7075 alloy and composites with 3, 6, and 9 wt.% TiB_2 reinforcement. SEM observations was used to examine the surface morphology and identify microstructural features, including cavities, local discontinuities, and possible defects. The corresponding SEM micrographs are presented in Figure 2.

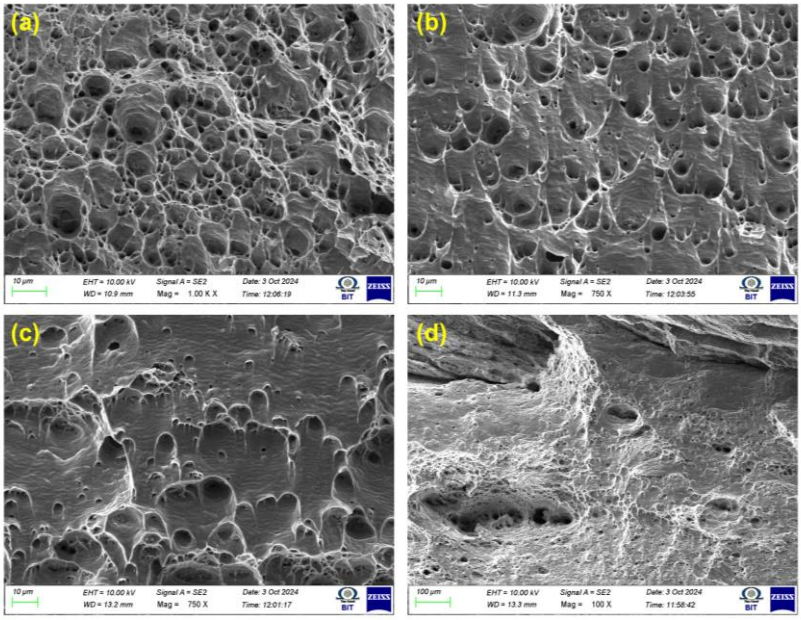

Fig. 2. SEM micrographs of (a) unreinforced AA7075 alloy, (b) AA7075/3 wt.% TiB_2, (c) AA7075/6 wt.% TiB_2, and (d) AA7075/9 wt.% TiB_2 composites.

The mechanical and tribological characteristics of fabricated AA7075/TiB_2 composites was analysed through tensile, hardness, and dry sliding wear tests. UTS were determined by universal testing machine, while hardness was evaluated using the Vickers indentation method. Dry sliding wear behaviour was assessed using a pin-on-disc testing arrangement. The tensile strength, hardness, and wear-rate results for the unreinforced alloy and TiB_2-reinforced composites are presented in Table 2.

Table 2. Mechanical and tribological properties of AA7075/TiB_2 composites.

Property	AA7075	AA7075/3% TiB_2	AA7075/6% TiB_2	AA7075/9% TiB_2
AA7075 (wt.%)	100	97	94	91
TiB_2 (wt.%)	0	3	6	9
UTS (MPa)	392.40	418.65	446.82	438.27
UTS improvement (%)	—	6.69	13.87	11.69
Hardness (HV)	132.60	148.35	163.72	175.48
Hardness improvement (%)	—	11.88	23.47	32.34
Wear rate ($\times 10^{-7}$ g/mm)	3.12	2.68	2.21	1.94
Wear-rate reduction (%)	—	14.10	29.17	37.82

The incorporation of TiB_2 particles influenced mechanical and tribological behaviour of AA7075 aluminium matrix composites. The unreinforced AA7075 alloy exhibited an ultimate tensile strength of 392.40 MPa, which increased to 418.65 MPa and 446.82 MPa with the addition of 3 and 6 wt.% TiB_2, respectively. The maximum tensile strength was obtained at 6 wt.% TiB_2, corresponding to an improvement of 13.87% compared with the unreinforced alloy. A subsequent reduction to 438.27 MPa was observed at 9 wt.% TiB_2, although the strength remained higher than that of the base alloy. This behaviour may be associated with

improved load transfer at moderate reinforcement concentrations and possible particle agglomeration or stress concentration at higher TiB_2 content.

Vickers hardness increased progressively from 132.60 HV for the unreinforced AA7075 alloy to 148.35, 163.72, and 175.48 HV for composites containing 3, 6, and 9 wt.% TiB_2, respectively. The highest hardness represented an improvement of 32.34%, indicating enhanced resistance to localized plastic deformation with increasing ceramic reinforcement. Similarly, the wear rate decreased from 3.12×10^{-7} g/mm for the unreinforced alloy to 1.94×10^{-7} g/mm at 9 wt.% TiB_2, corresponding to a reduction of 37.82%. The improvement in wear resistance may be attributed to the increased hardness and load-bearing contribution of the TiB_2 particles. These results demonstrate that TiB_2 incorporation modifies the mechanical and wear characteristics of AA7075 composites, providing basis for evaluating their subsequent friction stir welding performance.

2.2. Identification of friction stir welding process parameters

The FSW process parameters were selected to investigate their influence on percentage elongation (PE), ultimate tensile strength (UTS) and weld nugget hardness (WNH) of AA7075/TiB_2 composite joints. Four independent factors was considered: welding speed (WS), tool rotational speed, TiB_2 reinforcement content and axial load. Tool rotational speed governs frictional heat generation and material plasticization, while welding speed influences heat input and material consolidation along the welding direction. Axial load controls the contact pressure between workpiece and rotating tool, affecting material flow and joint formation. Additionally, TiB_2 reinforcement content was incorporated as an independent factor to examine addition of ceramic particles at mechanical characteristics of the welded composites.

A non-consumable rotating tool consist of shoulder and protruding pin was employed for friction stir welding. The rotating pin promotes mechanical stirring and transportation of plasticized material, whereas the shoulder contributes to frictional heating and consolidation of the weld region. The tool configuration was maintained constant throughout the experimental trials to evaluate addition of selected process parameters at mechanical performance of joints. The FSW tool used in the present investigation is shown in Figure 3.



Fig. 3. Friction stir welding tool pin used for joining AA7075/TiB_2 composites.

2.3. Selection of friction stir welding process parameter limits

The operating ranges of the selected FSW parameters were established to investigate effects of welding conditions at mechanical properties of AA7075/TiB_2 composite joints. The experimental factors comprised welding speed, tool rotational speed, TiB_2 reinforcement content, and axial load. Each factor was assigned three levels to develop experimental design by Taguchi L27 orthogonal array.

Tool rotational speed was varied between 900 and 1300 rpm, with an intermediate level of 1100 rpm. Welding speed was selected at 30, 50, and 70 mm/min, while axial load was varied from 3 to 7 kN at intervals of 2 kN. The TiB_2 reinforcement concentrations were maintained at 3, 6, and 9 wt.%, corresponding to the fabricated AA7075/TiB_2 composite compositions. The selected parameters, notations, units, and experimental levels are presented in Table 3.

Table 3. Friction stir welding process parameters and their experimental levels.

S. No.	Process parameter	Notation	Unit	Level 1	Level 2	Level 3
1	Tool rotational speed	TRS (A)	rpm	900	1100	1300
2	Welding speed	WS (B)	mm/min	30	50	70
3	Axial load	AL (C)	kN	3	5	7
4	TiB_2 reinforcement content	TiB_2 (D)	wt.%	3	6	9

For statistical representation, the lower, intermediate, and upper levels of each process parameter were designated as −1, 0, and +1, respectively. The relationship between the actual and coded values was expressed as:

$$X_i = \frac{Z_i - Z_{0i}}{\Delta Z_i} \tag{1}$$

where X_i represents the coded value of the selected factor, Z_i denotes its actual experimental value, Z_{0i} is the central value, and ΔZ_i represents the difference between the central and lower levels.

2.4. Development of Taguchi experimental design

Taguchi design of experiments were used to systematically investigate effects of four independent factors on the mechanical performance of FSW AA7075/TiB_2 composites. Each factor was considered at three levels, resulting in a full factorial requirement of 81 experimental combinations. To reduce the number of experimental trials while maintaining an orthogonal arrangement of factor levels, a Taguchi L27 orthogonal array consisting of 27 experimental runs was selected.

The experimental design was developed using Minitab software. The four factors were assigned to the orthogonal array, and the welding trials were arranged according to the selected combinations of welding speed, tool rotational speed, TiB_2 content, and axial load. Measured responses comprised percentage elongation, weld nugget hardness and ultimate tensile strength. Experimental design matrix and corresponding mechanical responses are presented in Table 4.

Table 4. Taguchi L27 experimental design matrix and mechanical responses of AA7075/TiB_2 FSW joints.

Run	TRS (rpm)	WS (mm/min)	AL (kN)	TiB_2 (wt.%)	UTS (MPa)	PE (%)	WNH (HV)

1	900	30	3	3	421.8	7.42	158.6
2	900	30	5	6	447.3	7.18	171.4
3	900	30	7	9	439.6	6.53	180.7
4	900	50	3	6	438.7	6.91	168.9
5	900	50	5	9	452.6	6.48	181.8
6	900	50	7	3	445.1	7.31	163.7
7	900	70	3	9	412.9	5.94	174.2
8	900	70	5	3	426.5	6.72	160.8
9	900	70	7	6	432.8	6.35	171.6
10	1100	30	3	6	462.4	7.61	174.3
11	1100	30	5	9	478.7	7.08	187.5
12	1100	30	7	3	469.5	7.84	168.1
13	1100	50	3	9	481.6	7.21	189.2
14	1100	50	5	3	486.8	8.46	172.7
15	1100	50	7	6	501.7	8.12	185.6
16	1100	70	3	3	451.3	7.36	165.9
17	1100	70	5	6	472.9	7.25	178.8
18	1100	70	7	9	466.4	6.62	190.4
19	1300	30	3	9	444.8	6.17	184.9
20	1300	30	5	3	456.7	7.03	166.8
21	1300	30	7	6	464.2	6.78	179.7
22	1300	50	3	3	458.5	7.12	167.6
23	1300	50	5	6	476.3	6.94	181.9
24	1300	50	7	9	468.1	6.21	193.2
25	1300	70	3	6	436.9	6.18	176.4
26	1300	70	5	9	447.6	5.82	188.7
27	1300	70	7	3	441.2	6.51	164.3

2.5. FSW experiments

The FSW was performed on the fabricated AA7075/TiB_2 composite plates using the selected process parameter combinations. The composite plates were positioned in a square butt-joint configuration and securely clamped to restrict movement during welding. The rotating tool was aligned with the joint interface, and the pin was gradually plunged into the workpieces under the specified axial load. Following the initial plunging operation, the tool traversed along the joint line at the predetermined welding speed.

During welding, frictional heating and mechanical stirring softened the surrounding aluminium matrix, allowing the plasticized material to flow at rotating pin and consolidate behind the tool. The welding speed, axial load and tool rotational speed, were varied to Taguchi L27 experimental design, while tool geometry was maintained constant. The welding procedure was repeated for the composite compositions containing 3, 6, and 9 wt.% TiB_2 according to the experimental matrix. Friction stir welding arrangement were illustrated in Figure 4.

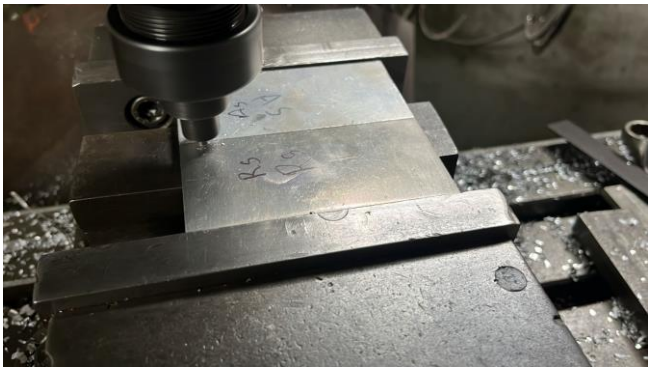

Fig. 4. Experimental arrangement for friction stir welding of AA7075/TiB_2 composite plates.

2.6. Evaluation of mechanical responses

Mechanical performance of friction stir welded joints was analysed in terms of percentage elongation, weld nugget hardness and ultimate tensile strength. Tensile specimens were prepared from the welded plates with the weld region positioned within the gauge section. Tensile testing were performed by universal testing machine to determine the maximum load sustained by the welded joints before fracture.

Ultimate tensile strength was calculated using Equation (2).

$$UTS = \frac{F_{\max}}{A_0} \tag{2}$$

where $F_{\max}$ is the maximum tensile load (N) and A_0 is the original cross-sectional area of the tensile specimen (mm^2).

Percentage elongation was determined from the change in gauge length after fracture using Equation (3).

$$PE = \frac{L_f - L_0}{L_0} \times 100 \tag{3}$$

where L_0 and L_f represent the initial and final gauge lengths, respectively. Weld nugget hardness was evaluated using the Vickers indentation method. Hardness measurements were taken within the stir zone to determine the resistance of the welded material to localized plastic deformation. The Vickers hardness number was determined using Equation (4).

$$HV = \frac{0.1891F}{d^2} \tag{4}$$

where F were applied indentation force in newtons and d were mean diagonal length of indentation in millimetres.

2.7. Taguchi signal-to-noise ratio analysis

Taguchi signal-to-noise (S/N) ratio were employed to analyse influence of welding parameters on selected mechanical responses. Since higher percentage elongation, tensile

strength, and nugget hardness were desirable, larger-the-better quality characteristic was adopted for all three responses. S/N ratio were calculated by Eqn (5) (Ogaili et al., 2026).

$$S/N = -10\log_{10}\left(\frac{1}{n}\sum_{i=1}^{n}\frac{1}{y_i^2}\right) \quad (5)$$

where n represents number of observations and y_i denotes measured response value.

S/N ratios were calculated for each experimental combination, and average S/N ratio at all factor level were determined. Main-effects plots were developed to identify the influence of welding speed, tool rotational speed, TiB_2 content and axial load on mechanical responses. Difference at maximum and minimum S/N ratios were used to analyse relative ranking of the process parameters.

2.8. ANOVA

ANOVA were perform to contribution of selected welding parameters to variations at UTS, PE, and WNH. Statistical analysis was carried out using Minitab software at a 95% confidence level. Significance of all factor was assessed by F-value and corresponding p-value, with p-values below 0.05 showing statistically significant effects.

Percentage contribution of all process parameter were calculated using Equation (6).

$$P_i = \frac{SS_i}{SS_T} \times 100 \quad (6)$$

where P_i represents the percentage contribution of selected factor, SS_i denotes its sum of squares, and SS_T represents total sum of squares.

An additive main-effects model were considered to describe relationship of process parameters and mechanical responses, as expressed in Equation (7).

$$Y_{ijkl} = \mu + A_i + B_j + C_k + D_l + \varepsilon_{ijkl} \quad (7)$$

where Y_{ijkl} represents the response, μ denotes the overall mean, A_i, B_j, C_k, and D_l represent the effects of welding speed, tool rotational speed, TiB_2 reinforcement content and axial load respectively, and ε_{ijkl} denotes the residual error.

The adequacy of the fitted models evaluated by coefficient of determination (R^2), adjusted R^2, predicted R^2, and residual analysis.

2.9. Prediction of optimum welding conditions

The optimum welding conditions were determined separately for UTS, PE, and WNH using the Taguchi S/N response analysis. The factor levels corresponding to the highest average S/N ratios were selected for each mechanical response. The predicted response at the selected optimum condition was calculated using the additive Taguchi model, as expressed in Equation (8).

$$\hat{Y}_{\text{opt}} = \bar{Y} + \sum_{i=1}^{k} \left(\bar{Y}_{i,\text{ opt}} - \bar{Y}\right) \quad (8)$$

where $\hat{Y}_{\text{opt}}$ is the predicted response at the optimum factor combination, $\bar{Y}$ represents the overall response mean, $\bar{Y}_{i,\text{ opt}}$ denotes the mean response at the selected optimum level of the i th factor, and k represents the number of factors.

The predicted optimum values were obtained separately for UTS, PE, and WNH because the most favourable TiB_2 reinforcement content and axial load were not identical for all three responses.

3. Results and Discussion

3.1. Taguchi response analysis

The influence of welding speed, tool rotational speed, TiB_2 reinforcement content and axial load on the percentage elongation, ultimate tensile strength, and weld nugget hardness of AA7075/TiB_2 FSW joints was investigated using Taguchi mean response and S/N ratio analyses. Larger-the-better quality properties were adopted for all three mechanical responses because higher tensile strength, elongation, and hardness were desirable. The mean response analysis was used to examine variations in mechanical properties across the selected parameter levels, whereas S/N ratio were employed to identify preferred welding conditions. Corresponding mean response values and S/N ratios are presented in Tables 5 and 6, respectively.

The mean response analysis revealed that tool rotational speed with greatest addition on UTS, followed by welding speed, axial load, and TiB_2 reinforcement content. As shown in Table 5, the mean UTS increased from 435.3 MPa at 900 rpm to 474.6 MPa at 1100 rpm, followed by a reduction to 454.9 MPa at 1300 rpm. Welding speed exhibited a similar trend, with the maximum mean UTS of 467.7 MPa occurring at 50 mm/min. The highest mean UTS values for axial load and TiB_2 content were 460.6 MPa at 5 kN and 459.2 MPa at 6 wt.%, respectively. The corresponding delta values were 39.3, 24.5, 15.2, and 8.4 MPa for TRS, WS, AL, and TiB_2 content. These outcomes show rotational speed was dominant parameter governing tensile strength within the investigated experimental range.

Percentage elongation also exhibited considerable sensitivity to tool rotational speed and reinforcement concentration. The mean PE increased from 6.760% at 900 rpm to 7.506% at 1100 rpm before decreasing to 6.529% at 1300 rpm. The maximum mean elongation of 7.196% was obtained at welding speed of 50 mm/min, while axial load of 5 kN produced highest mean value of 6.996%. Increasing TiB_2 content from 3 to 9 wt.% reduced the mean PE from 7.308% to 6.451%, indicating a reduction in ductility with increasing ceramic reinforcement. The delta values for TRS, TiB_2 content, WS, and AL were 0.977, 0.857, 0.668, and 0.116, respectively. Accordingly, TRS ranked first, followed by TiB_2 content, welding speed, and axial load.

In contrast, TiB_2 reinforcement content exerted the greatest influence on weld nugget hardness. The mean WNH increased from 165.4 HV at 3 wt.% TiB_2 to 176.5 HV at 6 wt.% and 185.6 HV at 9 wt.%. Tool rotational speed also affected hardness, with the highest mean value of 179.2 HV recorded at 1100 rpm. The maximum mean WNH values corresponding to welding

speed and axial load were 178.3 HV at 50 mm/min and 177.5 HV at 7 kN, respectively. The delta values were 20.2 HV for TiB_2 content, 9.0 HV for TRS, 4.2 HV for AL, and 3.7 HV for WS. The pronounced increase in hardness with TiB_2 concentration may be associated with the resistance offered by ceramic particles to localized plastic deformation.

Table 5. Taguchi mean response and ranking of FSW process parameters for UTS, PE, and WNH.

Response	Parameter	Level 1	Level 2	Level 3	Delta	Rank
UTS (MPa)	TRS	435.3	474.6	454.9	39.3	1
	WS	453.9	467.7	443.2	24.5	2
	AL	445.4	460.6	458.7	15.2	3
	TiB_2	450.8	459.2	454.7	8.4	4
PE (%)	TRS	6.760	7.506	6.529	0.977	1
	WS	7.071	7.196	6.528	0.668	3
	AL	6.880	6.996	6.919	0.116	4
	TiB_2	7.308	7.036	6.451	0.857	2
WNH (HV)	TRS	170.2	179.2	178.2	9.0	2
	WS	174.7	178.3	174.6	3.7	4
	AL	173.3	176.7	177.5	4.2	3
	TiB_2	165.4	176.5	185.6	20.2	1

S/N ratio were performed to analyse factor levels associated with improved mechanical performance. For UTS, the S/N ratios at the three rotational speed levels were 52.77, 53.52, and 53.16 dB, respectively, with the highest value occurring at 1100 rpm. The S/N delta for TRS was 0.75, followed by WS (0.47), AL (0.29), and TiB_2 content (0.16). The highest S/N ratios for all four factors occurred at their second levels. Therefore, the preferred parameter combination for maximizing UTS was A2B2C2D2, corresponding to 1100 rpm, 50 mm/min, 5 kN, and 6 wt.% TiB_2.

For percentage elongation, the S/N delta values were 1.21 for TRS, 1.08 for TiB_2 content, 0.83 for WS, and 0.14 for AL. The corresponding influence ranking was TRS > TiB_2 > WS > AL. The maximum S/N ratios were obtained at the second levels of WS, TRS, and AL and first level of TiB_2 content. Thus, the preferred combination for maximizing PE was A2B2C2D1, representing 1100 rpm, 50 mm/min, 5 kN, and 3 wt.% TiB_2. The preference for lower reinforcement content is consistent with the reduction in mean elongation observed as TiB_2 concentration increased.

The S/N response for weld nugget hardness exhibited a different parameter ranking. TiB_2 content showed the highest delta of 1.00, followed by TRS (0.44), AL (0.20), and WS (0.18). The highest S/N ratios were associated with the second levels of TRS and WS and the third levels of AL and TiB_2 content. Accordingly, A2B2C3D3 was identified as the preferred combination for maximizing WNH, corresponding to 1100 rpm, 50 mm/min, 7 kN, and 9 wt.% TiB_2. The increasing hardness response with TiB_2 concentration indicates the substantial contribution of ceramic reinforcement to indentation resistance within the weld nugget region.

Table 6. Taguchi S/N response and ranking of FSW process parameters for UTS, PE, and WNH.

Response	Parameter	Level 1	Level 2	Level 3	Delta	Rank
UTS	TRS	52.77	53.52	53.16	0.75	1
	WS	53.13	53.39	52.92	0.47	2
	AL	52.97	53.26	53.22	0.29	3

	TiB_2	53.07	53.23	53.15	0.16	4
PE	TRS	16.58	17.49	16.28	1.21	1
	WS	16.97	17.10	16.27	0.83	3
	AL	16.72	16.86	16.76	0.14	4
	TiB_2	17.25	16.92	16.17	1.08	2
WNH	TRS	44.61	45.05	45.00	0.44	2
	WS	44.83	45.01	44.83	0.18	4
	AL	44.77	44.93	44.97	0.20	3
	TiB_2	44.37	44.93	45.37	1.00	1

The main-effects plot for S/N ratios and means, presented in Figures 5–7, indicated that welding speed of 50 mm/min and tool rotational speed of 1100 rpm were the preferred conditions for all three mechanical responses. However, the optimum axial load and TiB_2 reinforcement content varied depending on the response considered. The highest predicted UTS was associated with an axial load of 5 kN and 6 wt.% TiB_2 (Figure 5), whereas PE was favoured by 5 kN and 3 wt.% TiB_2 (Figure 6). In contrast, WNH was maximized at 7 kN and 9 wt.% TiB_2 (Figure 7). These variations indicate that tensile strength, ductility, and hardness respond differently to the selected welding parameters, supporting the separate determination of optimum factor combinations for each mechanical response. In previous work, AA7075 aluminium matrix composites containing 0–15 wt.% TiO_2 were developed using stir casting to investigate dry sliding wear characteristics. Taguchi L16 grey relational analysis revealed reinforcement percentage as the most significant parameter affecting wear rate and coefficient of friction, followed by applied load (Alagarsamy et al., 2022)

3.2. Analysis of variance and model adequacy

ANOVA were used to relative contribution of all parameter to response variation. Results for UTS showed that TRS were dominant parameter with contribution of 60.87%, followed as WS at 23.83%, AL at 10.76%, and TiB_2 reinforcement content at 2.80%. The residual contribution was limited to 1.74%. All four parameters were statistically significant for UTS with $p < 0.001$.

For PE, TRS again exhibited the largest contribution at 43.27%, followed by TiB_2 content at 31.82% and WS at 20.94%. AL contributed only 0.57% and was statistically insignificant ($p = 0.245$), while the remaining three parameters were significant at $p < 0.001$. The residual contribution of 3.39% indicates that most of the observed PE variation was accounted for by the selected parameters.

The WNH response was predominantly controlled by TiB_2 reinforcement content, which accounted for 73.83% of the variation. TRS contributed 17.41%, while AL and WS contributed 3.50 and 3.23%, respectively. All four factors were significant at $p < 0.001$, and the residual contribution was only 2.03%. The pronounced contribution of TiB_2 indicates that reinforcement content was considerably more influential on local hardness than changes in WS or AL.

Table 7. ANOVA outcomes for UTS, PE, and WNH.

Response	Source	DF	Seq. SS	Contribution (%)	Adj. MS	F-value	p-value
UTS	TRS	2	6962.0	60.87	3481.00	314.17	<0.001
	WS	2	2725.3	23.83	1362.67	122.98	<0.001
	AL	2	1231.2	10.76	615.60	55.56	<0.001
	TiB_2	2	319.9	2.80	159.93	14.43	<0.001

	Error	18	199.4	1.74	11.08	–	–
PE	TRS	2	4.6894	43.27	2.34471	114.77	<0.001
	WS	2	2.2699	20.94	1.13494	55.55	<0.001
	AL	2	0.0622	0.57	0.03111	1.52	0.245
	TiB_2	2	3.4487	31.82	1.72434	84.40	<0.001
	Error	18	0.3677	3.39	0.02043	–	–
WNH	TRS	2	435.74	17.41	217.868	77.02	<0.001
	WS	2	80.96	3.23	40.478	14.31	<0.001
	AL	2	87.52	3.50	43.760	15.47	<0.001
	TiB_2	2	1848.31	73.83	924.156	326.69	<0.001
	Error	18	50.92	2.03	2.829	–	–

The statistical adequacy of the fitted models was further evaluated from the coefficients of determination. The UTS model produced an R^2 of 98.26%, adjusted R^2 of 97.48%, and predicted R^2 of 96.08%. Corresponding values for PE were 96.61, 95.10, and 92.37%, respectively, while the WNH model exhibited R^2, adjusted R^2, and predicted R^2 values of 97.97**,** 97.06, and 95.42%, respectively. The relatively small differences between adjusted and predicted R^2 indicate consistent fitting and prediction within the investigated factor space. In earlier research, Al 8009 aluminium alloy reinforced with varying TiB_2 contents was fabricated using ultrasonic probe-assisted stir casting. A 5 wt.% TiB_2 composite achieved a maximum tensile strength of 127 MPa and hardness of 128.39 HV. ANOVA confirmed significant predictive models with R^2 values of 0.9658 and 0.9980 for coefficient of friction and specific wear rate (Gowthami & Vemula, 2025).

Table 8. Statistical adequacy of the fitted response models.

Response	S	R^2 (%)	Adjusted R^2 (%)	Predicted R^2 (%)
UTS	3.32868	98.26	97.48	96.08
PE	0.142932	96.61	95.10	92.37
WNH	1.68193	97.97	97.06	95.42

3.3. Effect of process parameters on UTS

The main-effects plot for UTS showed a pronounced dependence on TRS. The mean UTS increased from 435.3 MPa at 900 rpm to 474.6 MPa at 1100 rpm, followed by a decrease to 454.9 MPa at 1300 rpm. The improvement up to 1100 rpm indicates that the increase in rotational speed promoted a more favourable thermomechanical condition within the weld region. Greater rotational action increases frictional heating and assists plasticized material movement around the tool, thereby improving consolidation. The subsequent reduction at 1300 rpm indicates that increasing rotational speed beyond the favourable level did not provide an additional strength benefit.

Welding speed produced mean UTS values of 453.9, 467.7, and 443.2 MPa at 30, 50, and 70 mm/min, respectively. Maximum response at 50 mm/min indicates that an intermediate welding speed provided a favourable balance between tool interaction time and heat input. Increasing WS to 70 mm/min shortened the interaction period and was accompanied by a pronounced decrease in UTS.

The corresponding mean UTS values at AL levels of 3, 5, and 7 kN were 445.4, 460.6, and 458.7 MPa, respectively. Increasing AL from 3 to 5 kN improved the tensile response, whereas further increase to 7 kN produced only a slight reduction. The intermediate AL

therefore provided sufficient forging action for effective material consolidation without producing an additional benefit at the highest level.

TiB_2 content had the smallest statistical contribution to UTS, although its response still showed a distinct intermediate optimum. The mean UTS increased from 450.8 MPa at 3 wt.% to 459.2 MPa at 6 wt.%, before lowering to 454.7 MPa at 9 wt.%. The improvement at 6 wt.% indicates a favourable contribution of the ceramic reinforcement to the load-bearing response, whereas the reduction at 9 wt.% shows that raising reinforcement content beyond intermediate level did not further improve tensile strength. The combined mean and S/N results consequently identify 1100 rpm, 50 mm/min, 5 kN, and 6 wt.% TiB_2 as the preferred factor levels for UTS. In previous work, Cr-Mo-V hot-work die steel was reinforced with 0.02 wt.% TiC–TiB_2 particles using an Al-based master alloy. Microstructural refinement reduced grain size from 17.6 to 15.4 µm and martensite-lath width from 0.38 to 0.31 µm. At 600 °C, yield strength increased from 601 to 655 MPa, while tensile strength improved from 659 to 724 MPa (Li et al., 2026).

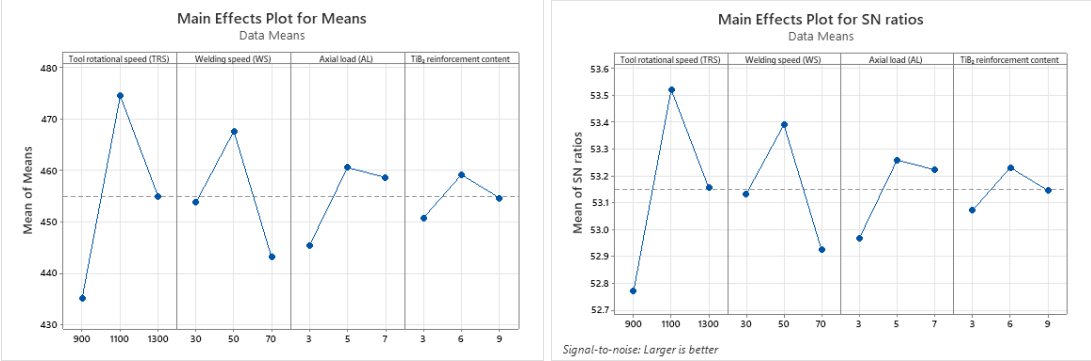

Fig. 5. Effect of welding speed, tool rotational speed, TiB_2 reinforcement content, and axial load on mean UTS and corresponding larger-the-better S/N ratio.

3.4. Effect of process parameters at elongation percentage

The PE response exhibited a strong dependence on TRS and TiB_2 content. The mean PE increased from 6.760% at 900 rpm to 7.506% at 1100 rpm and then decreased to 6.529% at 1300 rpm. The maximum ductility at the intermediate rotational speed indicates that 1100 rpm provided a more favourable thermomechanical condition for retaining plastic deformation capability within the joint.

Increasing WS from 30 to 50 mm/min resulted in a modest increase in mean PE from 7.071 to 7.196%. A further increase to 70 mm/min reduced PE to 6.528%. Thus, the intermediate welding speed was favourable for elongation, whereas the highest welding speed caused a substantial reduction.

The mean PE changed only marginally with AL, recording 6.880, 6.996, and 6.919% at 3, 5, and 7 kN, respectively. This limited variation agrees with the ANOVA result, where AL accounted for only 0.57% of the total response variation and was statistically insignificant. Within the selected range, alteration of AL therefore produced no substantial change in joint elongation.

A clear reduction in PE occurred with increasing TiB_2 content. Mean elongation decreased from 7.308% at 3 wt.% to 7.036% at 6 wt.% and 6.451% at 9 wt.%. Rigid TiB_2 reinforcement restricts deformation of the aluminium matrix, resulting in reduced elongation

as its fraction increases. This trend differs from the hardness response and demonstrates the mechanical trade-off associated with increasing ceramic reinforcement. Based on the larger-the-better S/N response, the preferred levels for PE were 1100 rpm, 50 mm/min, 5 kN, and 3 wt.% TiB_2. In earlier investigation, Al-Si/Mg_2Si hybrid composites reinforced with 0–5 wt.% TiB_2 were fabricated using cooling slope casting. The incorporation of TiB_2 reduced α-Al grain size by 51% and refined Mg_2Si morphology by 46%. The optimum 5 wt.% TiB_2 composite exhibited a 55% increase in percentage elongation, 28% improvement in tensile strength, and 30% enhancement in hardness (Yadav et al., 2023).

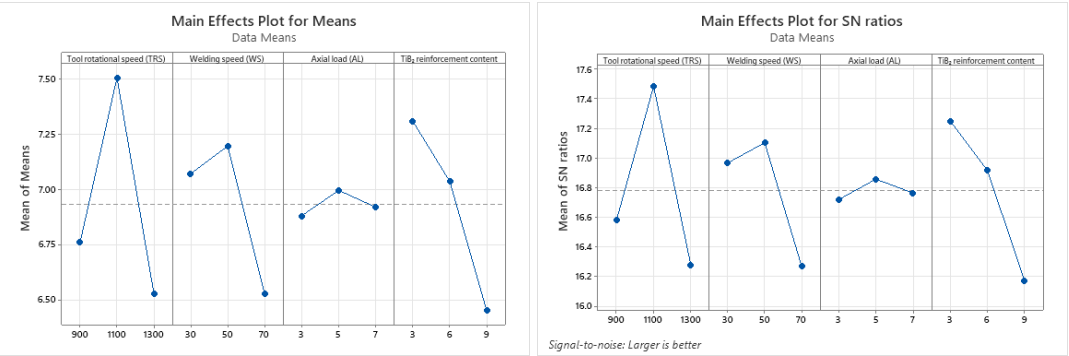

Fig. 6. Effect of welding speed, tool rotational speed, TiB_2 reinforcement, and axial load content on the mean percentage elongation and corresponding larger-the-better S/N ratio.

3.5. Influence of process parameters on weld nugget hardness

WNH showed the strongest dependence on TiB_2 reinforcement content. The mean hardness increased from 165.4 HV at 3 wt.% to 176.5 HV at 6 wt.% and 185.6 HV at 9 wt.%. Increase from 3 to 9 wt.% corresponded to approximately 12.2% improvement in mean WNH. The trend is consistent with the ANOVA contribution of 73.83%, confirming TiB_2 content as the primary factor controlling hardness.

The improvement can be associated with the presence of hard TiB_2 particles within the aluminium matrix, which increases resistance to localized plastic deformation. The reinforcement can also impede deformation of the surrounding matrix during indentation. Consequently, unlike the UTS response, WNH continued to increase up to the highest TiB_2 level considered.

The mean WNH increased from 170.2 HV at 900 rpm to 179.2 HV at 1100 rpm, followed by a slight decrease to 178.2 HV at 1300 rpm. TRS was therefore the second most influential factor, accounting for 17.41% of the total variation. The response indicates that the thermomechanical conditions generated at 1100 rpm were favourable for developing a harder weld nugget.

WS produced mean WNH values of 174.7, 178.3, and 174.6 HV at 30, 50, and 70 mm/min, respectively. AL produced values of 173.3, 176.7, and 177.5 HV at 3, 5, and 7 kN. Although both parameters were statistically significant, their percentage contributions were relatively small compared with TiB_2 and TRS. Based on the S/N response, the preferred condition for maximizing WNH was 1100 rpm, 50 mm/min, 7 kN, and 9 wt.% TiB_2. In earlier work, Dissimilar AA5083-O and AA7075-T6 aluminium alloys were joined using friction stir welding (FSW) with process parameters optimized through RSM. The optimum rotational speed of 1100 rpm, welding speed of 50 mm/min, and tool tilt angle of 2° achieved a weld hardness of 189 HV0.1, tensile strength of 417 MPa, and weld efficiency of 80.65%.

Microstructural analysis revealed refined nugget-zone grains of 0.3–0.7 μm (Mothilal & Kumar, 2024)

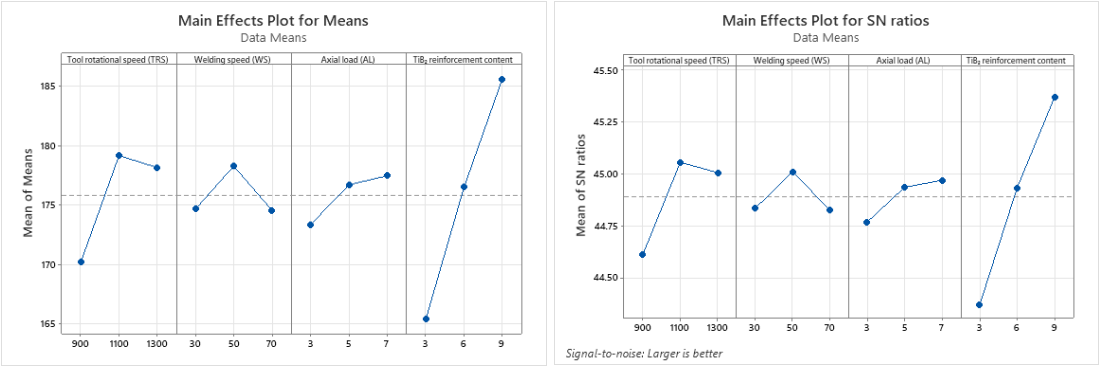

Fig. 7. Effect of welding speed, tool rotational speed, TiB_2 and axial load, reinforcement content on the mean weld nugget hardness and corresponding larger-the-better S/N ratio.

3.6. Residual analysis

Residual diagnostics were examined to assess the statistical behaviour of the fitted models. The normal probability plots for UTS, PE, and WNH showed that the majority of residual points followed the reference line without pronounced systematic departure. The residual-versus-fitted plots showed residuals distributed on both sides of zero without an evident funnel-shaped pattern. The residual-versus-order plots also showed fluctuations around the zero reference without a progressive response trend. These observations support the overall adequacy of the fitted models for representing the experimental responses.

The Minitab diagnostics identified observations 10 and 15 for UTS**,** 14 and 15 for PE, and 27 for WNH as unusual observations based on comparatively large standardized residuals. For UTS, observations 10 and 15 had standardized residuals of −2.20 and 2.28, respectively. For PE, observations 14 and 15 showed standardized residuals of 2.14 and 2.22, whereas observation 27 for WNH exhibited a standardized residual of −2.75. These observations represent localized deviations rather than a general residual pattern and should be retained unless an experimental or recording error is independently established.

The high R^2 values and comparatively close adjusted and predicted R^2 values further support the statistical consistency of the models. In particular, predicted R^2 remained above 92% for all three responses, indicating that the fitted effects retained good predictive capability within the investigated experimental domain. In previous study, AA7075 aluminium alloy reinforced with 0–9 wt.% SiC was investigated for wear behavior under varying loads, sliding velocities, and distances. Machine learning models achieved $R^2 \approx 0.89$ and RMSE ≈ 0.0009 after optimization. Residual analysis revealed unbiased, approximately normally distributed errors (Kunduru, 2026).

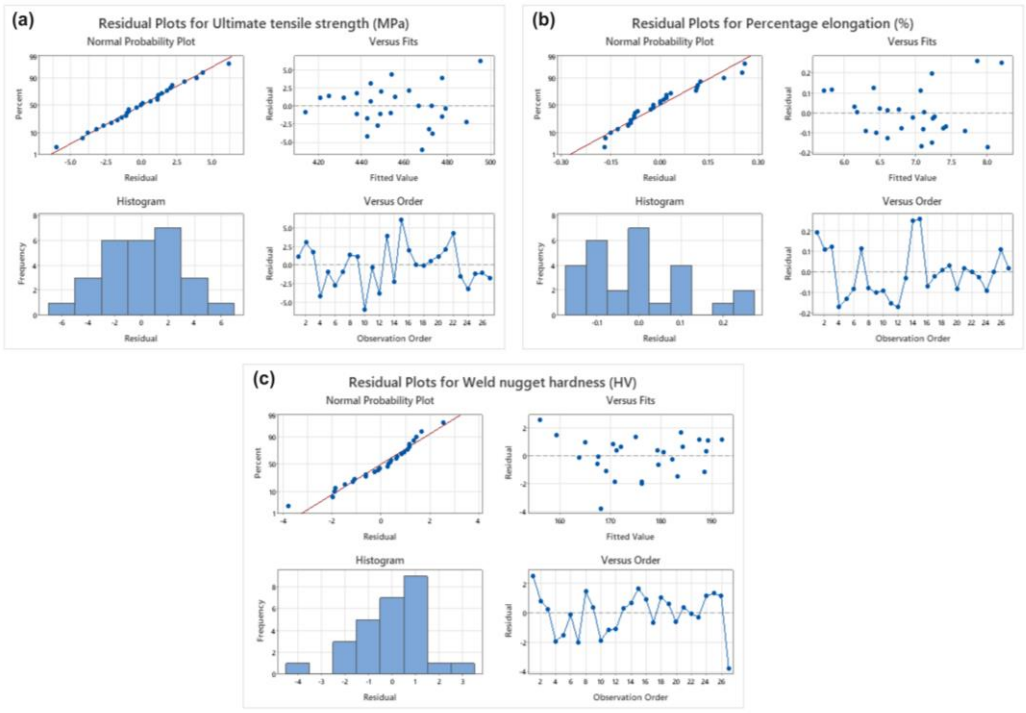

Fig. 8. Residual diagnostic plots for (a) UTS, (b) Elongation percentage, and (c) nugget hardness.

3.7. Comparative influence of the process parameters

Comparison of the ANOVA contributions reveals that the relative importance of the FSW parameters depended strongly on the selected mechanical response. For UTS, the order of contribution was TRS (60.87%) > WS (23.83%) > AL (10.76%) > TiB_2 (2.80%). For PE, the order changed to TRS (43.27%) > TiB_2 (31.82%) > WS (20.94%) > AL (0.57%). WNH showed a substantially different response, with the order TiB_2 (73.83%) > TRS (17.41%) > AL (3.50%) > WS (3.23%).

Table 9. Comparative contribution and ranking of process parameters.

Response	Rank 1	Rank 2	Rank 3	Rank 4	Error
UTS	TRS (60.87%)	WS (23.83%)	AL (10.76%)	TiB_2 (2.80%)	1.74%
PE	TRS (43.27%)	TiB_2 (31.82%)	WS (20.94%)	AL (0.57%)	3.39%
WNH	TiB_2 (73.83%)	TRS (17.41%)	AL (3.50%)	WS (3.23%)	2.03%

The comparison indicates that TRS predominantly governed the tensile characteristics, whereas TiB_2 content exerted the greatest influence on hardness. The response of PE also demonstrates the competing role of reinforcement: increasing TiB_2 markedly increased WNH but progressively reduced elongation. Therefore, the factor level producing the maximum value of one mechanical response cannot be assumed to provide simultaneous optimization of all three responses. In earlier investigation, AA7075-T6 aluminium alloy was investigated using friction stir welding (FSW) with flat-shouldered and scrolled-shoulder threaded tools at rotational speeds of 1100–1700 rpm and welding speeds of 70–120 mm/min. Increasing rotational speed raised peak temperature by 250°C, while higher welding speed reduced it by 100–130°C. At 1320 rpm and 70 mm/min (TOUMI et al., 2026).

3.8. Selection of optimum parameter levels

The optimum parameter levels for PE, UTS, and WNH was determined independently from the larger-the-better S/N response. The analysis revealed that the preferred parameter levels varied according to the mechanical response considered. However, welding speed (WS) of 50 mm/min and tool rotational speed (TRS) of 1100 rpm were consistently identified as the optimum levels for all three responses.

For UTS, the maximum S/N ratios were obtained at the second level of all four parameters, resulting in the optimum combination A2B2C2D2. This combination corresponds to TRS of 1100 rpm, axial load (AL) of 5 kN, WS of 50 mm/min, and TiB_2 content of 6 wt.%. For PE, the optimum combination was A2B2C2D1, corresponding to 1100 rpm, 50 mm/min, 5 kN, and 3 wt.% TiB_2. In contrast, WNH was favoured by the combination A2B2C3D3, representing 1100 rpm, 50 mm/min, 7 kN, and 9 wt.% TiB_2.

Table 10. Optimum factor levels obtained from the larger-the-better S/N analysis.

Response	TRS (rpm)	WS (mm/min)	AL (kN)	TiB_2 (wt.%)	Optimum combination
UTS	**1100**	**50**	**5**	**6**	**A2B2C2D2**
PE	**1100**	**50**	**5**	**3**	**A2B2C2D1**
WNH	**1100**	**50**	**7**	**9**	**A2B2C3D3**

The response-specific optimum conditions were consistent with trends obtained from main-effects and ANOVA results. For UTS, the intermediate TiB_2 content of 6 wt.% was preferred, whereas PE was favoured by the lower reinforcement content of 3 wt.%. In contrast, WNH reached its optimum at the highest TiB_2 content of 9 wt.%. This difference is also reflected in the ANOVA results, where TiB_2 accounted for 2.80% of the UTS variation, 31.82% of the PE variation, and 73.83% of the WNH variation**.**

Although TRS and WS exhibited common optimum levels for all three responses, the preferred AL and TiB_2 levels varied depending on the mechanical response. Therefore, the Taguchi analysis identified response-specific optimum parameter combinations for maximizing UTS, PE, and WNH individually. In earlier research, AA7075 aluminium alloy was coated using plasma electrolytic oxidation (PEO) and optimized through the Taguchi method. Frequency was the dominant parameter, achieving a maximum polarization resistance of $2332 \times 10^3\ \Omega\ cm^2$, approximately 476 times higher than the uncoated alloy (Songur et al., 2022).

3.9. Prediction and confirmation of optimum responses

The response values corresponding to the individual optimum parameter combinations were estimated using the fitted Taguchi response models. For UTS, the optimum combination A2B2C2D2 resulted in a predicted tensile strength of 497.38 MPa. For PE, the optimum combination A2B2C2D1 yielded a predicted elongation of 8.21%, whereas the optimum combination A2B2C3D3 for WNH resulted in a predicted hardness of 193.03 HV. These results demonstrate that the optimum conditions were response dependent, particularly with respect to AL and TiB_2 content.

Confirmation experiments at the respective optimum parameter combinations can be used to verify predictive capability of Taguchi models. Agreement between the predicted and experimentally measured responses can subsequently be evaluated from the percentage

deviation. Close agreement between these values would support the reliability of the identified optimum parameter levels.

Table 11. Predicted responses at the individual Taguchi optimum conditions.

Response	Optimum combination	Optimum parameter condition	Predicted response
UTS	**A2B2C2D2**	1100 rpm, 50 mm/min, 5 kN, 6 wt.% TiB_2	**497.38 MPa**
PE	**A2B2C2D1**	1100 rpm, 50 mm/min, 5 kN, 3 wt.% TiB_2	**8.21%**
WNH	**A2B2C3D3**	1100 rpm, 50 mm/min, 7 kN, 9 wt.% TiB_2	**193.03 HV**

The predicted responses indicate that the Taguchi optimization provided distinct parameter combinations for achieving the maximum value of each mechanical property. The common selection of 1100 rpm TRS and 50 mm/min WS indicates the importance of intermediate processing levels for the three responses, while adjustment of AL and TiB_2 content allows the processing condition to be selected according to the required tensile strength, ductility, or weld nugget hardness.

3.10. Macrostructural and microstructural analysis

The macrostructural and microstructural characteristics of the FSW AA7075/TiB_2 composite were shown in Fig. 9. The macrostructural examination revealed a distinct weld region formed by the combined effects of frictional heating and mechanical stirring during FSW. The weld cross-section exhibited visible differences between the central stirred region and the surrounding material, reflecting the nonuniform thermal and deformation conditions experienced during welding. A localized discontinuity was also observed within the weld region, suggesting the possible occurrence of incomplete material consolidation.

The optical micrographs revealed variations in microstructural morphology across the examined regions. These differences may be attributed to the combined influence of thermal exposure, plastic deformation, and material flow at FSW. The weld nugget zone is generally subjected to intense thermomechanical deformation, which can promote dynamic recrystallization and grain refinement, whereas the adjacent thermo-mechanically affected and heat-affected regions experience different combinations of deformation and heating. The observed morphological variations therefore indicate the influence of FSW processing on the microstructural characteristics of the AA7075/TiB_2 composite joints. However, quantitative grain-size measurements would be required to confirm the extent of grain refinement. In previous study, Microstructural refinement of AA7075-T6 aluminium alloy was achieved through friction stir processing using a square-profiled tool. Optimized processing at 1050 rpm and 60 mm/min produced a minimum grain size of 3.49 μm, maximum hardness of 147.1 HV, and tensile strength of 432 MPa (Girish, 2023).

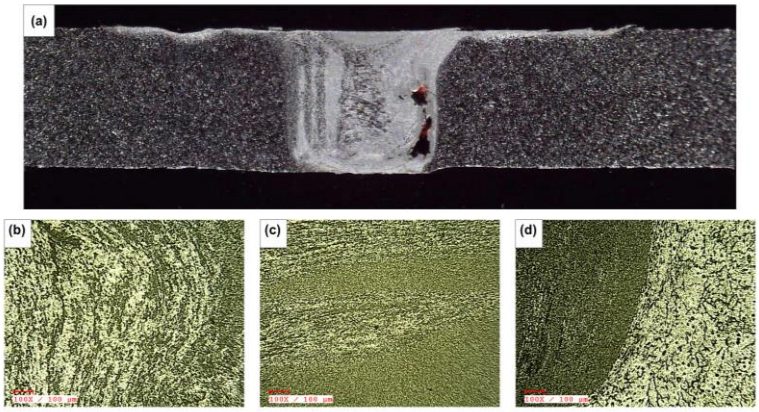

Fig. 9. (a) Macrostructural cross-section and (b–d) optical micrographs of different regions of the FSW AA7075/TiB_2 composite joint.

SEM micrographs of the AA7075/TiB_2 composite and FSW region were shown in Fig. 10. The micrographs reveal distinct morphological characteristics between the examined regions. Figure 10(a) exhibits a comparatively smooth surface with limited visible microstructural features, whereas Fig. 10(b) displays a heterogeneous morphology characterized by elongated structures and numerous bright particle-like features. These morphological differences may be associated with variations in local deformation, material flow, and reinforcement distribution during friction stir welding. However, confirmation of the chemical identity and distribution of TiB_2 particles requires additional compositional analysis.

The mechanical response analysis demonstrated that TiB_2 reinforcement content significantly influenced weld nugget hardness. The mean WNH increased from 165.4 HV at 3 wt.% TiB_2 to 176.5 HV at 6 wt.% and 185.6 HV at 9 wt.%. Furthermore, ANOVA identified TiB_2 content as the dominant factor governing WNH, contributing 73.83% of the total variation. In contrast, the Taguchi analysis indicated that 6 wt.% TiB_2 was preferred for maximizing UTS, whereas 3 wt.% TiB_2 favoured percentage elongation. These findings demonstrate the response-dependent addition of reinforcement concentration on mechanical efficiency of AA7075/TiB_2 friction stir welded joints. The SEM observations provide complementary morphological information, although a direct relationship between individual microstructural features and mechanical properties requires further characterization.

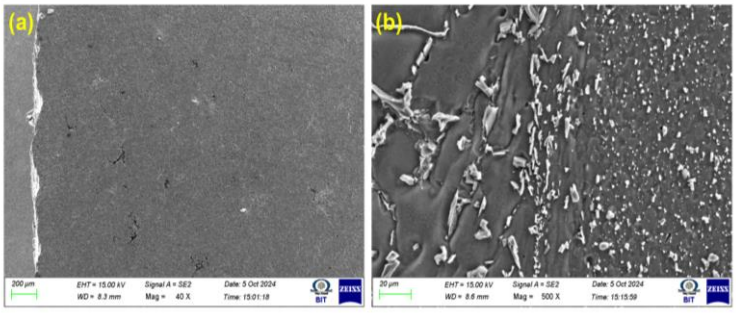

Fig. 10. SEM micrographs showing the surface morphology of (a) AA7075/TiB_2 composite (b) FSW AA7075/TiB_2 composite region.

4. Conclusion

The present reach investigated influence of FSW process parameters on mechanical performance of AA7075/TiB_2 aluminium matrix composites using a Taguchi L27 orthogonal array. Welding speed (30–70 mm/min), tool rotational speed (900–1300 rpm), TiB_2 reinforcement content (3–9 wt.%) and axial load (3–7 kN) were considered as independent factors, while percentage elongation (PE), weld nugget hardness (WNH)and ultimate tensile strength (UTS) was evaluated as mechanical responses. The Taguchi S/N ratio analysis and ANOVA was employed to determine relative influence of selected factors and identify the preferred welding conditions.

The results demonstrated that tool rotational speed was the dominant factor influencing UTS and PE, contributing 60.87% and 43.27% of their total variations, respectively. Welding speed contributed 23.83% to UTS and 20.94% to PE, while TiB_2 reinforcement content accounted for 31.82% of the variation in PE. In contrast, weld nugget hardness was predominantly governed by TiB_2 content, with a contribution of 73.83%, followed by tool rotational speed at 17.41%. The ANOVA results confirmed that all four factors significantly influenced UTS and WNH, whereas axial load exhibited no statistically significant effect on PE ($p = 0.245$). The fitted main-effects models exhibited R^2 values of 98.26%, 96.61%, and 97.97% for UTS, PE, and WNH, respectively, indicating strong agreement between the experimental responses and model estimates.

The Taguchi analysis identified A2B2C2D2 (1100 rpm, 50 mm/min, 5 kN, and 6 wt.% TiB_2) as the preferred parameter combination for maximizing UTS, with a predicted value of 497.38 MPa. The preferred condition for PE was A2B2C2D1 (1100 rpm, 50 mm/min, 5 kN, and 3 wt.% TiB_2), producing a predicted elongation of 8.21%. For WNH, the preferred combination was A2B2C3D3 (1100 rpm, 50 mm/min, 7 kN, and 9 wt.% TiB_2), with a predicted hardness of 193.03 HV. Although rotational speed of 1100 rpm and welding speed of 50 mm/min was favourable for all three responses, the preferred axial load and reinforcement concentration varied with the mechanical property considered. Overall, the findings shows effectiveness of Taguchi approach for evaluating parameter sensitivity and identifying response-specific welding conditions for AA7075/TiB_2 composites. The developed statistical models provide a basis for selecting FSW parameters within the investigated experimental ranges.

References

Abouhabaga, O., & El Shrief, E. (2026). Data-driven optimization of friction stir welding parameters of AA7075 aluminium alloy using ANN surrogates and genetic algorithms. *Beni-Suef University Journal of Basic and Applied Sciences*, *15*(1). https://doi.org/10.1186/s43088-026-00755-w

Agrawal, A. P., & Srivastava, S. K. (2024a). Investigating the Effects of Adding Si3N4 on Microstructural and Mechanical Characteristics of AA7075-based TiB2-Reinforced Hybrid MMCs. *International Journal of Metalcasting*, *18*(3), 2545–2561. https://doi.org/10.1007/s40962-023-01193-5

Agrawal, A. P., & Srivastava, S. K. (2024b). Synthesis, characterization, and mechanical properties of Al–Zn–Mg alloy-based hybrid metalmatrix composites reinforced with Si3N4/TiB2 particles processed through stir casting technique. *Proceedings of the*

Institution of Mechanical Engineers, Part L: Journal of Materials: Design and Applications, *238*(6), 1021–1037. https://doi.org/10.1177/14644207231207939

Alagarsamy, S. V, Ravichandran, M., & Meignanamoorthy, M. (2022). Multi-objective optimisation of dry sliding wear control parameters for stir casted AA7075- TiO2 composites using Taguchi-Grey relational approach. *Australian Journal of Mechanical Engineering*, *20*(5), 1453–1462. https://doi.org/10.1080/14484846.2020.1815997

Alam, M. I., & Singh, N. K. (2026). Optimization of wear parameters for developed aluminium hybrid composite AA7075/SiC/WC. *Engineering Research Express*, *8*(13). https://doi.org/10.1088/2631-8695/ae812f

Bhushan, R. K. (2023). GA approach for optimization of parameters in machining Al alloy SiC particle composite for minimum cutting force. *Journal of Alloys and Metallurgical Systems*, *1*. https://doi.org/10.1016/j.jalmes.2023.100002

Chen, S., Chen, H., Wang, G., Qiu, Z., Zheng, Z., Zeng, D., Zhu, D., Tang, X., Shi, R., & Wang, J. (2026). Microstructure and mechanical properties of (AlCoCrFeNi2.1 + TiB2) reinforced AlSi10Mg matrix composites fabricated via laser powder bed fusion. *Materials Science and Engineering: A*, *973*. https://doi.org/10.1016/j.msea.2026.150665

Chinnathambi, R., Uthirapathi, E., T, B., & S, S. (2026). Experimental investigation and empirical modeling of EDM performance and mechanical properties of in-situ synthesized A356-TiB2 composite using Box–Behnken based RSM. *Phosphorus, Sulfur and Silicon and the Related Elements*. https://doi.org/10.1080/10426507.2026.2714229

Cholkar, A., Chatterjee, S., McCann, R., McCarthy, É., Kinahan, D., & Brabazon, D. (2026). Ultrafast laser–material interactions in commercial aluminium alloys: Ablation threshold, material removal mechanisms, and surface chemistry under femtosecond laser irradiation. *Applied Surface Science Advances*, *35*. https://doi.org/10.1016/j.apsadv.2026.101057

Dey, D., Bhowmik, A., & Biswas, A. (2022). Tribological performance Optimization of Al2024-TiB2 composites using Grey-Taguchi approach. *International Journal of Cast Metals Research*, *35*(5–6), 144–151. https://doi.org/10.1080/13640461.2022.2149361

Girish, G. (2023). Tailoring surface properties of aerospace-grade aluminium alloy through solid-state friction stir processing. *Proceedings of the Institution of Mechanical Engineers, Part L: Journal of Materials: Design and Applications*, *237*(3), 577–591. https://doi.org/10.1177/14644207221119755

Gowthami, G., & Vemula, J. (2025). Fabrication and wear analysis of Al 8009-TiB2 composites produced by ultrasonic assisted stir casting. *International Journal on Interactive Design and Manufacturing*, *19*(8), 5601–5620. https://doi.org/10.1007/s12008-024-02152-y

Keskin, G., Salunkhe, S., Küçüktürk, G., Pul, M., Gürün, H., & Baydaroğlu, V. (2025). Optimization of PMEDM process parameters for B4C and B4C+SiC reinforced AA7075 composites. *Journal of Engineering Research (Kuwait)*, *13*(1), 47–56. https://doi.org/10.1016/j.jer.2023.09.012

Kunduru, V. R. (2026). Influence of hyperparameter optimization on the predictive accuracy of supervised machine learning models for the wear behavior of AA7075/SiC microwave

sintered composites. *Russian Physics Journal*, *69*(2), 173–184. https://doi.org/10.1007/s11182-026-03700-7

Li, C.-D., Dong, B.-X., Chen, P.-D., Qiu, F., Shu, S.-L., Chang, F., Yang, H.-Y., & Jiang, Q.-C. (2026). Enhanced short-term creep resistance of hot-work die steel via nanoparticle-assisted through-process microstructural regulation. *Materials Science and Engineering: A*, *976*. https://doi.org/10.1016/j.msea.2026.151047

Manikandan, R., Elatharasan, G., Parthiban, A., Sakthivel, T. G., Gopalakrishnan, T., & Raju, R. (2025). Experimental and computational analysis of thermal and mechanical characteristics in friction stir welding of dissimilar aluminum alloys with varying tool pin geometries. *Welding in the World*, *69*(7), 2003–2029. https://doi.org/10.1007/s40194-025-01975-x

Mothilal, M., & Kumar, A. (2024). Optimization of friction stir welding process parameter in the joining of AA7075-T6/AA5083-O dissimilar aluminum alloy using response surface methodology. *International Journal of Pressure Vessels and Piping*, *211*. https://doi.org/10.1016/j.ijpvp.2024.105282

Ogaili, A. A. F., Jweri, A.-R. K., Amin, S. A., & Jaber, A. A. (2026). Influence of lattice-core geometry on the mechanical performance of FDM-printed PETG sandwich panels: an experimental, computational, and statistical investigation. *Journal of Engineering and Applied Science*, *73*(1). https://doi.org/10.1186/s44147-026-01164-7

Puleo, R., Adnan, M., Ingarao, G., & Fratini, L. (2026). An improved upcycling approach for producing bimetallic tube via friction stir extrusion of aluminium chips. *International Journal of Advanced Manufacturing Technology*, *144*(5–6), 4279–4293. https://doi.org/10.1007/s00170-026-18114-5

Rong, Z., Yang, H., Rong, X., Zhang, X., Zhao, D., He, C., & Zhao, N. (2027). Grain boundary segregation engineering via in-situ TiB2 formation for enhanced mechanical properties in additively manufactured AA2024 alloys. *Journal of Materials Science and Technology*, *286*, 160–170. https://doi.org/10.1016/j.jmst.2026.08.013

Senthilkumar, C., Shanmugaelango, K., Nandakumar, C., & Elaiyarasan, U. (2026). Wear Performance and Its Examination of Electro-discharge Alloyed WS2/Cu Composite Coating on AA7075 Aluminium Alloy. *Journal of Bio- and Tribo-Corrosion*, *12*(3). https://doi.org/10.1007/s40735-026-01173-2

Sharma, B. M., Saraswat, P., Singh, H. R., Marwal, V. S., & Sharma, D. K. (2026a). Optimization of MIG welding parameters to maximize penetration in aluminium 7075 alloys. *Materials Research Express*, *13*(13). https://doi.org/10.1088/2053-1591/ae82c1

Sharma, B. M., Saraswat, P., Singh, H. R., Marwal, V. S., & Sharma, D. K. (2026b). Optimization of MIG welding parameters to maximize penetration in aluminium 7075 alloys. *Materials Research Express*, *13*(13). https://doi.org/10.1088/2053-1591/ae82c1

Songur, F., Arslan, E., & Dikici, B. (2022). Taguchi optimization of PEO process parameters for corrosion protection of AA7075 alloy. *Surface and Coatings Technology*, *434*. https://doi.org/10.1016/j.surfcoat.2022.128202

Suhas, B. G., Chidanand, K. M., Kiran Kumar, K. U., & Umesh, G. L. (2025). Study on Mechanical and Tribological Characterization of Titanium Diboride (TiB2) Reinforced Al7075 Composites by Taguchi Technique. *Journal of Materials and Engineering Structures*, *12*(2), 139–154. https://www.scopus.com/pages/publications/105033485302?origin=resultslist

TOUMI, O., HANNACHI, N., PRISCO, U., & ENNETTA, R. (2026). Thermal behaviour and material flow in FSW of high-strength aluminium alloys: Role of tool design and process conditions. *Sadhana - Academy Proceedings in Engineering Sciences*, *51*(3). https://doi.org/10.1007/s12046-026-03308-0

Türkkan, Y. A. (2026). Effect of pinless tool geometry and process parameters on the mechanical performance and microstructural evolution of friction stir spot welded AA7075-T6. *Materialpruefung/Materials Testing*, *68*(9), 1620–1631. https://doi.org/10.1515/mt-2026-0064

Yadav, A. K., Gautam, G., & Mohan, S. (2023). Microstructure-Mechanical Property Correlation in Cooling Slope Cast Al-Si/Mg2Si-xwt.% TiB2 (x = 0, 1, 3 and 5) insitu Hybrid Composites. *Silicon*, *15*(17), 7431–7440. https://doi.org/10.1007/s12633-023-02587-0